

# On columnar thin films as platforms for surface-plasmonic-polaritonic optical sensing: higher-order considerations

Siti S. Jamaian<sup>a</sup> and Tom G. Mackay<sup>a,b,1</sup>

<sup>a</sup>School of Mathematics and Maxwell Institute for Mathematical Sciences, University of Edinburgh, Edinburgh EH9 3JZ, UK

<sup>b</sup>NanoMM — Nanoengineered Metamaterials Group  
Department of Engineering Science and Mechanics, Pennsylvania State University,  
University Park, PA 16802-6812, USA

## Abstract

The ability to tailor the porosity and optical properties of columnar thin films (CTFs) renders them promising platforms for optical sensing. In particular, surface-plasmon-polariton (SPP) waves, guided by the planar interface of an infiltrated CTF and a thin layer of metal, may be harnessed to detect substances that penetrate the void regions in between the columns of a CTF. This scenario was investigated theoretically using a higher-order homogenization technique, based on an extended version of the second-order strong-permittivity-fluctuation theory, which takes into account the size of the component particles which make up the infiltrated CTF and the statistical distribution of these particles. Our numerical studies revealed that as the size of the component particles increases and as the correlation length that characterizes their distribution increases: (i) the phase speed of the SPP wave decreases and the SPP wave's attenuation increases; (ii) the SPP wave's penetration into the CTF decreases; (iii) the angle of incidence required to excite the SPP wave in a modified Kretschmann configuration increases; (iv) the sharpness of the SPP trough in the graph of reflectance versus angle of incidence increases; and (v) the sensitivity to changes in refractive index of the infiltrating fluid decreases.

**Keywords:** Surface plasmon polariton, columnar thin film, strong-permittivity-fluctuation theory, Bruggeman formalism

## 1 Introduction

A columnar thin film (CTF) consists of a parallel array of columnar nanowires, oriented at angle  $\chi$  to a planar substrate [1]. The columns may be grown on the substrate by means of physical vapour deposition. Through judicious control of the vapour deposition process, both the macroscopic optical properties and the porosity of the CTF can be tailored to order [2]. Consequently, CTFs are promising candidates as platforms for optical sensing applications, wherein it is envisaged that the species to be sensed is contained within a fluid which penetrates the void regions in between the CTF's columns.

A recent theoretical investigation highlighted the fact that surface-plasmon-polariton (SPP) waves, guided by the planar interface of an infiltrated CTF and a thin layer of metal, may be usefully harnessed for optical sensing [3]. In this scenario, the angle of incidence required to excite an SPP wave was found to be acutely sensitive to changes in refractive index  $n_\ell$  of the fluid which fills the CTF's void regions. Furthermore, the phase speed and propagation length of the SPP wave were also sensitive to  $n_\ell$ .

---

<sup>1</sup>E-mail: T.Mackay@ed.ac.uk.

A crucial step in modelling CTFs — as well as more general sculptured thin films — as platforms for such optical sensing is the estimation of the effective permittivity dyadic of the infiltrated CTF [4]. This may be achieved in a two-step homogenization process: First, an inverse homogenization procedure can be implemented to estimate certain nanoscale parameters (namely, refractive index, shape parameter and volume fraction) for the uninfiltrated CTF, using experimentally-determined values of the uninfiltrated CTF’s permittivity dyadic [5]. Second, a forward homogenization approach can then be used to estimate the effective permittivity dyadic of the infiltrated CTF. In recent studies the well-established Bruggeman homogenization formalism was employed for this purpose [3, 6, 7]. However, there are certain limitations with the Bruggeman formalism. It does not take into account the nonzero size of particles which make up the component materials nor does it take into account the statistical distribution of these component particles. But both the size and distribution of the component particles can have a significant bearing upon the estimates provided by homogenization formalisms. For example, significant higher-order effects associated with the nonzero size of component particles were recently reported for a homogenization study based on an infiltrated chiral sculptured thin film [8].

In the following we investigate CTFs as platforms for SPP optical sensing using a higher-order approach to homogenization, based on the strong-permittivity-fluctuation theory (SPFT) [9]. A second-order implementation is used wherein the statistical distributions of the component particles are characterized in terms of a two-point correlation function and its correlation length  $L$  [10, 11, 12]. Also, an extended implementation is used wherein the nonzero size of component particles is accommodated via a size parameter  $\eta$  which originates from the corresponding depolarization dyadics [13]. Two SPP scenarios are investigated: (i) a canonical scenario wherein the SPP wave is guided by the planar interface of a CTF half-space and a metal half-space (Sec. 3); and (ii) a realistic scenario for SPP wave excitation based on a modification of the Kretschmann configuration (Sec. 4). Our particular goal is to elucidate the effects of the higher-order homogenization parameters  $L$  and  $\eta$  on SPP wave excitation. As the theory which underpins our study is described comprehensively elsewhere, we provide only a brief outline of the theory (along with appropriate citations to the recent literature) before presenting our numerical results.

As regards notation, vectors are written in boldface while  $3 \times 3$  dyadics are underlined twice. The unit vectors  $\mathbf{u}_x$ ,  $\mathbf{u}_y$  and  $\mathbf{u}_z$  are aligned with the Cartesian  $x$ ,  $y$  and  $z$  axes. The real and imaginary parts of complex quantities are provided by the operators  $\text{Re}[\cdot]$  and  $\text{Im}[\cdot]$ ; and  $i = \sqrt{-1}$ . An  $\exp(-i\omega t)$  time-dependence is implicitly assumed, with  $\omega$  being the angular frequency and  $t$  being time. The free-space wavenumber is denoted as  $k_0$ .

## 2 Homogenization

### 2.1 Macroscopic perspective

Macroscopically, a CTF may be regarded as a homogeneous biaxial dielectric material, characterized by a relative permittivity dyadic of the form [1, 2]

$$\underline{\underline{\epsilon}}_{ctf\nu} = \epsilon_{a\nu} \mathbf{u}_n \mathbf{u}_n + \epsilon_{b\nu} \mathbf{u}_\tau \mathbf{u}_\tau + \epsilon_{c\nu} \mathbf{u}_b \mathbf{u}_b, \quad (\nu = 1, 2). \quad (1)$$

Herein  $\nu = 1$  denotes an uninfiltrated CTF and  $\nu = 2$  an infiltrated CTF, while the normal, tangential and binormal basis vectors are given by

$$\left. \begin{aligned} \mathbf{u}_n &= -\mathbf{u}_x \sin \chi + \mathbf{u}_z \cos \chi \\ \mathbf{u}_\tau &= \mathbf{u}_x \cos \chi + \mathbf{u}_z \sin \chi \\ \mathbf{u}_b &= -\mathbf{u}_y \end{aligned} \right\} \quad (2)$$

with the column inclination angle  $\chi \in (0, \pi/2]$ . The permittivity parameters for certain uninfiltated CTFs have been experimentally determined. For example,

$$\left. \begin{aligned} \epsilon_{a1} &= \left[ 1.0443 + 2.7394 \left( \frac{2\chi_v}{\pi} \right) - 1.3697 \left( \frac{2\chi_v}{\pi} \right)^2 \right]^2 \\ \epsilon_{b1} &= \left[ 1.6765 + 1.5649 \left( \frac{2\chi_v}{\pi} \right) - 0.7825 \left( \frac{2\chi_v}{\pi} \right)^2 \right]^2 \\ \epsilon_{c1} &= \left[ 1.3586 + 2.1109 \left( \frac{2\chi_v}{\pi} \right) - 1.0554 \left( \frac{2\chi_v}{\pi} \right)^2 \right]^2 \end{aligned} \right\} \quad (3)$$

for a CTF made from patinal<sup>®</sup> titanium oxide, as determined at a free-space wavelength of 633 nm [14]. Here  $\chi_v$  is the angle of incidence of the vapour flux during the deposition process used to fabricate the CTF. It is related to the column inclination angle  $\chi$  via

$$\tan \chi = 2.8818 \tan \chi_v. \quad (4)$$

For definiteness, we fix  $\chi_v = 30^\circ$ . From a knowledge of  $\{\epsilon_{a1}, \epsilon_{b1}, \epsilon_{c1}\}$ , the corresponding permittivity parameters for a CTF infiltrated by a fluid of refractive index  $n_\ell$ , namely  $\{\epsilon_{a2}, \epsilon_{b2}, \epsilon_{c2}\}$ , can be estimated using an inverse/forward homogenization process, as we now describe.

## 2.2 Nanostructural perspective

Within our homogenization approach, the columns of the CTF are envisaged at the nanoscale as assemblies of ellipsoidal particles, all with their major axes aligned with the rotational axis of the columns. Thus, the surface of each ellipsoidal particle, relative to its centre, is prescribed by the position vector

$$\eta \underline{\underline{U}} \cdot \hat{\mathbf{r}}, \quad (5)$$

where  $\hat{\mathbf{r}}$  is the radial unit vector which prescribes the surface of the unit sphere. In conformity with eq. (1), the shape dyadic  $\underline{\underline{U}}$  has the form

$$\underline{\underline{U}} = \frac{1}{\sqrt{\gamma_\tau \gamma_b}} (\mathbf{u}_n \mathbf{u}_n + \gamma_\tau \mathbf{u}_\tau \mathbf{u}_\tau + \gamma_b \mathbf{u}_b \mathbf{u}_b). \quad (6)$$

A suitably elongated ellipsoidal shape is achieved by choosing the shape parameters  $\gamma_b \gtrsim 1$  and  $\gamma_\tau \gg 1$ . The value  $\gamma_\tau = 15$  is selected here because larger values of  $\gamma_\tau$  do not result in any significant effects for slender inclusions [15]. The size parameter  $\eta$  provides a measure of the linear dimensions of the ellipsoidal particle. In compliance with the homogenization regime,  $\eta$  must be smaller than the wavelengths involved, but it need not be vanishingly small. In conventional homogenization formalisms, as typified by the Bruggeman formalism, the limit  $\eta \rightarrow 0$  is taken, whereas in extended formalisms nonzero values of  $\eta$  are incorporated [16].

The regions in between the columns of the CTFs (whether infiltrated or not) are taken to have the same particulate nanonstructure as the columns themselves. So that there are no spaces in between the ellipsoidal component particles, a fractal-like distribution of the component particles is envisaged. Accordingly, the size parameter  $\eta$  should be regarded as an upper bound on the linear dimensions of the component particles [17].

In conventional homogenization formalisms, as typified by the Bruggeman formalism, the distributions of the component materials are characterized solely in terms of volume fraction: therein, the volume fraction of a CTF occupied by columns is  $f \in (0, 1)$ , while  $1 - f$  is the volume fraction not occupied by columns. In addition to volume fraction, the second-order SPFT also characterises the distribution of the component materials in terms of a two-point correlation function and its associated correlation length  $L$  [9, 12]. The

wavelengths involved are presumed to be large in relation to the correlation length. Furthermore, on the grounds of physical reasonableness, the inequality  $L > \eta$  should be satisfied [13].

The deposited material from which the columns of the CTF are composed is assumed to be an isotropic dielectric material of refractive index  $n_s$ . This refractive index is generally somewhat different to the refractive index of the bulk material that was evaporated to make the CTF, depending upon the precise details of the deposition environment [18, 19].

We emphasize that the nanoscale parameters  $\{\gamma_b, f, n_s\}$  are not readily determined by direct measurement. Therefore, we rely upon theoretical estimates of these quantities.

### 2.3 Inverse homogenization — uninfiltated CTF

The first step towards the estimation of the infiltrated CTF's permittivity parameters  $\{\epsilon_{a2}, \epsilon_{b2}, \epsilon_{c2}\}$  involves an application of inverse homogenization. The (nonextended) Bruggeman formalism is inverted to yield estimates of the shape parameter  $\gamma_b$ , volume fraction  $f$  and refractive index  $n_s$ , making use of the experimentally-determined values of  $\{\epsilon_{a1}, \epsilon_{b1}, \epsilon_{c1}\}$  provided in eqs. (3) for the uninfiltated CTF. This procedure is described in detail elsewhere [5]. Parenthetically, certain constitutive parameter regimes are known to be problematic for the inverse Bruggeman formalism [20] (and, indeed, also problematic for the forward Bruggeman formalism [21]) but these regimes are not the same as those considered here.

### 2.4 Forward homogenization — infiltrated CTF

The second step towards the estimation of the infiltrated CTF's permittivity parameters  $\{\epsilon_{a2}, \epsilon_{b2}, \epsilon_{c2}\}$  involves combining the estimated nanoscale parameters  $\{\gamma_b, f, n_s\}$  with the refractive index of the infiltrating fluid  $n_\ell$  in an application of forward homogenization. In contrast with recent studies, we implement an extended version of the second-order SPFT for this purpose. Thereby, the distributional statistics of the component materials as well as the nonzero size of the component particles are taken into account. A full description of the extended version of the second-order SPFT — appropriate to biaxial homogenized composite materials, based on oriented ellipsoidal component particles, precisely as is the case here — is available elsewhere [13, 17]. Let us note that in the limits  $L \rightarrow 0$  and  $\eta \rightarrow 0$ , the nonextended, zeroth-order SPFT emerges which is equivalent to the Bruggeman formalism. Also, higher-order homogenization approaches such as those implemented here generally do not scale in a physically-intuitive manner [22], but the physical significance of this aspect is unclear.

Numerical estimates of  $\epsilon_{a2}$ ,  $\epsilon_{b2}$  and  $\epsilon_{c2}$ , as computed using the extended version of the second-order SPFT, are plotted against  $\eta/L \in (0, 1)$  and  $k_0 L \in (0, 0.2)$  in Fig. 1. To allow direct comparison with an earlier study based on the Bruggeman formalism [3], the refractive index of the fluid infiltrating the void regions of the CTF was fixed at  $n_\ell = 1.5$ . The real parts of  $\{\epsilon_{a2}, \epsilon_{b2}, \epsilon_{c2}\}$  increase modestly, but significantly, as both  $L$  and  $\eta$  increase. More conspicuous is the uniform increase in the imaginary parts of  $\{\epsilon_{a2}, \epsilon_{b2}, \epsilon_{c2}\}$  from the null values that they take in the limits  $L \rightarrow 0$  and  $\eta \rightarrow 0$ . The emergence of these nonzero imaginary parts is indicative of losses due to scattering from the macroscopic coherent field [23]. These scattering losses increase as the component particles increase in size and as the correlation length increases. Such scattering losses are a general feature of higher-order approaches to homogenization, arising whenever the component materials are characterized by a (nonzero) length scale [24, 25].

## 3 Canonical boundary-value problem

Now we turn to the excitation of SPP waves, guided by the planar interface of a CTF half-space and metal half-space. This scenario allows us to explore the wavenumbers of the SPP waves and thereby consider the phase speeds and propagation lengths of the SPP waves. The theory for this canonical boundary-value problem was developed recently by Lakhtakia and Polo [26].

Let assume that a metal of relative permittivity  $\epsilon_m$  occupies the half-space  $z < 0$  while a CTF infiltrated by a fluid of refractive index  $n_\ell$  occupies the half-space  $z > 0$ . We consider the  $p$ -polarized SPP wave which

is guided by the planar interface. The electric field phasor of the SPP wave may be expressed as [26]

$$\mathbf{E}(\mathbf{r}) = \begin{cases} A_m \left( \mathbf{u}_x - \frac{i\sigma}{q_m} \mathbf{u}_z \right) \exp [ik_0 (\sigma x - iq_m z)], & z < 0 \\ A_c \left[ \mathbf{u}_x + \frac{i\sigma q_c - (\epsilon_{a2} - \epsilon_{b2}) \sin \chi \cos \chi}{\sigma^2 - (\epsilon_{a2} \cos^2 \chi + \epsilon_{b2} \sin^2 \chi)} \mathbf{u}_z \right] \exp [ik_0 (\sigma x + iq_c z)], & z > 0 \end{cases}, \quad (7)$$

where  $A_m$  and  $A_c$  are the complex-valued amplitudes,  $\sigma k_0 \mathbf{u}_x$  represents the wave vector of the SPP wave, and  $q_m = \sqrt{\sigma^2 - \epsilon_m}$ . The relative wavenumber  $\sigma$  and  $q_c$  are deduced from the corresponding dispersion relations. The roots of the dispersion relations are chosen such that  $\text{Re} [q_{m,c}] > 0$ , thereby ensuring that the SPP wave decays in directions normal to the interface  $z = 0$ .

For our numerical studies we chose  $\epsilon_m = -56 + 21i$  (which is the value for bulk aluminium at a free-space wavelength of 633 nm), in keeping with previous studies [3]. In Fig. 2, the real and imaginary parts of  $\sigma$  are plotted against  $\eta/L \in (0, 1)$  and  $k_0 L \in (0, 0.2)$ . The real part of  $\sigma$  increases uniformly as both the correlation length and the size parameter increase. Accordingly, a significant decrease in the phase speed of the SPP wave may be inferred as both  $L$  increases and  $\eta$  increases. As the imaginary part of  $\sigma$  similarly increases in a uniform fashion as both the correlation length and the size parameter increase, we deduce that attenuation of the SPP wave is significantly increased upon increasing both  $L$  and  $\eta$ .

Next we turn to the penetration of the SPP wave into the CTF in the  $+z$  direction. An inverse measure of this is provided by  $\text{Re} [q_c]$ , which is plotted against  $\eta/L$  and  $k_0 L$  in Fig. 3. Thus, from Fig. 3 we deduce that SPP wave penetration into the CTF decreases as the correlation length increases and as the size parameter increases.

## 4 Modified Kretschmann configuration

The Kretschmann configuration [27] represents a realistic scenario for SPP wave excitation. A modification of this configuration is considered here [28], guided by experimental views for launching surface waves [29], wherein a fluid-infiltrated CTF of finite thickness occupies the region  $L_m < z < L_\Sigma$  and a thin metal film occupies the region  $0 < z < L_m$ . The region  $z > L_\Sigma$  is filled by a dielectric material with relative permittivity  $\epsilon_\ell = n_\ell^2$ , while the region  $z < 0$  is filled by a dielectric material with relative permittivity  $\epsilon_d$ .

Suppose that a  $p$ -polarized plane wave propagates in the region  $z \leq 0$  towards the metal-coated CTF at an angle  $\theta_{inc} \in (0, \pi/2)$  to the  $+z$  axis. This incident plane wave gives rise to a reflected plane wave in the  $z < 0$  region and a transmitted plane wave in the  $z > L_\Sigma$  region. Thus, the corresponding electric field phasors in the regions above and below the metal-coated CTF may be expressed as [3, 26]

$$\mathbf{E} = \begin{cases} (-\mathbf{u}_x \cos \theta_{inc} + \mathbf{u}_z \sin \theta_{inc}) \exp [i (\kappa x + \sqrt{\epsilon_d} z \cos \theta_{inc})] \\ + r_p (\mathbf{u}_x \cos \theta_{inc} + \mathbf{u}_z \sin \theta_{inc}) \exp [i (\kappa x - \sqrt{\epsilon_d} z \cos \theta_{inc})], & z < 0 \\ t_p (-\mathbf{u}_x \cos \theta_{tr} + \mathbf{u}_z \sin \theta_{tr}) \exp [i (\kappa x + \sqrt{\epsilon_\ell} (z - L_\Sigma) \cos \theta_{tr})], & z > L_\Sigma \end{cases}, \quad (8)$$

wherein the angles of incidence and transmission are related by

$$\sqrt{\epsilon_d} \sin \theta_{inc} = \sqrt{\epsilon_\ell} \sin \theta_{tr} \equiv \sigma \quad (9)$$

and  $\kappa = k_0 \sigma$ . By solving the associated boundary value-problem, the complex-valued reflection and transmission coefficients, namely  $r_p$  and  $r_t$ , are determined.

We may identify the excitation of a SPP wave at the metal-CTF interface via the reflectance  $|r_p|^2$  or the absorbance

$$A_p = 1 - (|r_p|^2 + \beta |t_p|^2), \quad (10)$$

wherein the scalar parameter

$$\beta = \frac{\sqrt{\epsilon_\ell} \text{Re} [\cos \theta_{tr}]}{\sqrt{\epsilon_d} \cos \theta_{inc}}. \quad (11)$$

A sharp trough in graph of  $|r_p|^2$  (or sharp peak in the graph of  $A_p$ ) versus  $\theta_{inc}$  is the characteristic signature of SPP-wave excitation, provided that  $\theta_{inc}$  is greater than the critical angle for total reflection in the absence of the metal film. In order to ensure the existence of this critical angle, in our numerical studies we chose  $\epsilon_d = 6.76$ , which is in the range of rutile.

A representative plot of the reflectance  $|r_p|^2$  versus  $\theta_{inc}$  is presented in Fig. 4 for  $k_0L = 0.2$  and  $\eta/L = 1$ . We set the thicknesses  $L_m = 10$  nm and  $L_\Sigma = L_m + 1000$  nm. Also plotted in this figure is  $\beta|t_p|^2$ . In the regime  $\theta_{inc} > 36^\circ$  (which corresponds to the total reflection regime in the absence of the metal film), the value of the absorbance  $A_p$  can be inferred from that of the reflectance  $|r_p|^2$  since  $\beta|t_p|^2$  is null-valued here. The rightmost local minimum in the graph of  $|r_p|^2$  (at  $\theta_{inc} = 70.8^\circ$ ) indicates the excitation of a SPP wave. The other local minimums in the graph of  $|r_p|^2$ , which occur for  $36^\circ < \theta_{inc} < 70.8^\circ$ , represent waveguide modes [30]. Crucially, these waveguide modes are excited at different values  $\theta_{inc}$  as the thickness of the CTF is varied, whereas the value of  $\theta_{inc}$  which excites the SPP wave is independent of the CTF's thickness (as we confirmed in numerical calculations not presented here).

Let us now focus on  $\theta_{inc}^\#$  which denotes the value of  $\theta_{inc}$  corresponding to the rightmost local minimum in the graph of  $|r_p|^2$  versus  $\theta_{inc}$ ; i.e., it corresponds to the value of  $\theta_{inc}$  at which the SPP wave is excited. The sensitivity of this angle  $\theta_{inc}^\#$  to the correlation length and size parameter is demonstrated in Fig. 5, where  $\theta_{inc}^\#$  is plotted against  $\eta/L \in (0, 1)$  and  $k_0L \in (0, 0.2)$ . We see that  $\theta_{inc}^\#$  increases uniformly as  $L$  increases and as  $\eta$  increases. In particular, the value of  $\theta_{inc}^\#$  for  $L = 0.2/k_0$  and  $\eta = L$  is approximately one degree greater than it is in the limits  $L \rightarrow 0$  and  $\eta \rightarrow 0$ .

From the point of view of sensing applications, the shape of the local minimum at  $\theta_{inc} = \theta_{inc}^\#$  is an important consideration. To explore the effects of the correlation length and size parameter on the shape of the SPP trough, the second derivative  $d^2(|r_p|^2)/d\theta_{inc}^2$  is plotted against  $\eta/L \in (0, 1)$  and  $k_0L \in (0, 0.2)$  in Fig. 6. We observe that the SPP trough becomes uniformly sharper as  $L$  increases, but changes relatively little as  $\eta$  increases. In particular, the SPP trough for  $L = 0.2/k_0$  and  $\eta = L$  is approximately 2% sharper than it is in the limits  $L \rightarrow 0$  and  $\eta \rightarrow 0$ .

Lastly, we turn to the sensitivity of the SPP trough in the graph of  $|r_p|^2$  versus  $\theta_{inc}$  to changes in the refractive index  $n_\ell$  of the fluid which infiltrates the CTF. A convenient measure of this sensitivity is provided by the figure of merit (in degree/RIU<sup>2</sup>) [3]

$$\rho = \frac{\theta_{inc}^\#(n_{\ell 2}) - \theta_{inc}^\#(n_{\ell 1})}{n_{\ell 2} - n_{\ell 1}}, \quad (12)$$

where  $\theta_{inc}^\#$  is regarded as function of  $n_\ell$ . For  $n_{\ell 2} = 1.5$  and  $n_{\ell 1} = 1.0$  the figure of merit is plotted against  $\eta/L \in (0, 1)$  and  $k_0L \in (0, 0.2)$  in Fig. 7. The sensitivity, as gauged by  $\rho$ , decreases uniformly as both the correlation length increases and as the size parameter increases. In particular, the sensitivity drops by approximately 4 degree/RIU as  $L$  and  $\eta$  both increase from zero to  $0.2/k_0$ .

## 5 Closing remarks

The potential that infiltrated CTFs offer for SPP-based optical sensing has been demonstrated in previous theoretical studies using the Bruggeman homogenization formalism. We have further elucidated this matter by implementing a more sophisticated homogenization approach based on the extended second-order SPFT which takes into account the statistical distribution of the component materials and the size of the component materials. Specifically, our numerical investigations have revealed that as the correlation length increases and as the size parameter increases:

- the phase speed of the SPP wave decreases and the SPP wave's attenuation increases;
- the SPP wave's penetration into the CTF decreases;

---

<sup>2</sup>RIU = refractive-index unit

- the angle of incidence required to excite the SPP wave in a modified Kretschmann configuration increases;
- the sharpness of the SPP trough in the graph of reflectance versus angle of incidence increases;
- and the sensitivity to changes in refractive index of the infiltrating fluid decreases.

As well as directly shedding further light on SPP-based CTF sensors, these results also highlight the importance of using higher-order homogenization methods when considering sculptured thin films generally as platforms for optical sensing. For example, in principle a similar higher-order homogenization approach could be usefully employed for chiral sculptured thin films, which are also promising candidates for SPP-based optical sensing [7].

**Acknowledgments:** SSJ is fully sponsored by Universiti Tun Hussein Onn Malaysia.

## References

- [1] A. Lakhtakia, R. Messier, *Sculptured Thin Films: Nanoengineered Morphology and Optics*, SPIE Press, Bellingham, WA, USA (2005).
- [2] G. B. Smith, Theory of angular selective transmittance in oblique columnar thin films containing metal and voids, *Appl. Opt.* 29 (1990) 3685–3693.
- [3] T. G. Mackay, A. Lakhtakia, Modeling columnar thin films as platforms for surface-plasmonic-polaritonic optical sensing, *Photon. Nanostruct. Fundam. Appl.* 8 (2010) 140–149.
- [4] J. A. Sherwin, A. Lakhtakia, I. J. Hodgkinson, On calibration of a nominal structure-property relationship model for chiral sculptured thin films by axial transmittance measurements, *Opt. Commun.* 209 (2002) 369–375.
- [5] T. G. Mackay, A. Lakhtakia, Determination of constitutive and morphological parameters of columnar thin films by inverse homogenization, *J. Nanophoton.* 4 (2010) 041535.
- [6] T. G. Mackay, A. Lakhtakia, Empirical model of optical sensing via spectral shift of circular Bragg phenomenon, *IEEE Photon. J.* 2 (2010) 92–101.
- [7] T. G. Mackay, A. Lakhtakia, Modeling chiral sculptured thin films as platforms for surface-plasmonic-polaritonic optical sensing, *IEEE Sens. J.* (at press) doi:10.1109/JSEN.2010.2067448.
- [8] S. S. Jamaian, T. G. Mackay, On chemiluminescent emission from an infiltrated chiral sculptured thin film, *Opt. Commun.* 284 (2011) 2382–2392. Erratum: 284 (2011) 3488–3489.
- [9] L. Tsang, J. A. Kong, Scattering of electromagnetic waves from random media with strong permittivity fluctuations, *Radio Sci.* 16 (1981) 303–320.
- [10] Z. D. Genchev, Anisotropic and gyrotropic version of Polder and van Santen’s mixing formula, *Waves Random Media* 2 (1992) 99–110.
- [11] N. P. Zhuck, Strong-fluctuation theory for a mean electromagnetic field in a statistically homogeneous random medium with arbitrary anisotropy of electrical and statistical properties, *Phys. Rev. B* 50 (1994) 15636–15645.



- [12] T. G. Mackay, A. Lakhtakia, W. S. Weiglhofer, Third-order implementation and convergence of the strong-property-fluctuation theory in electromagnetic homogenisation, *Phys. Rev. E* 64 (2001) 066616.
- [13] T. G. Mackay, Depolarization volume and correlation length in the homogenization of anisotropic dielectric composites, *Waves Random Media* 14 (2004) 485–498. Erratum: *Waves Random Complex Media* 16 (2006) 85.
- [14] I. Hodgkinson, Q. h. Wu, J. Hazel, Empirical equations for the principal refractive indices and column angle of obliquely deposited films of tantalum oxide, titanium oxide, and zirconium oxide, *Appl. Opt.* 37 (1998) 2653–2659.
- [15] A. Lakhtakia, Enhancement of optical activity of chiral sculptured thin films by suitable infiltration of void regions, *Optik* 112 (2001) 145–148. Erratum: 112 (2001) 544.
- [16] T. G. Mackay, A. Lakhtakia, Electromagnetic fields in linear bianisotropic mediums, *Prog. Opt.* 51 (2008) 121–209.
- [17] T. G. Mackay, Effective constitutive parameters of linear nanocomposites in the long-wavelength regime, *J. Nanophoton.* 5 (2011) 051001.
- [18] F. Walbel, E. Ritter, and R. Linsbod, “Properties of  $\text{TiO}_x$  films prepared by electron-beam evaporation of titanium and titanium suboxides,” *Appl. Opt.* 42 (2003) 4590–4593.
- [19] H. A. Macleod, *Thin-Film Optical Filters*, 3rd ed., Institute of Physics, Bristol, UK (2001).
- [20] S. S. Jamaian, T. G. Mackay, On limitations of the Bruggeman formalism for inverse homogenization, *J. Nanophoton.* 4 (2010) 043510.
- [21] T. G. Mackay, A. Lakhtakia, A limitation of the Bruggeman formalism for homogenization, *Opt Commun.* 234 (2004) 35–42. Erratum: 282 (2009) 4028.
- [22] C. F. Bohren, Do extended effective-medium formulas scale properly?, *J. Nanophoton.* 3 (2009) 039501.
- [23] J. Van Kranendonk, J. E. Sipe, Foundations of the macroscopic electromagnetic theory of dielectric media, *Prog. Opt.* 15 (1977) 245–350.
- [24] W. T. Doyle, Optical properties of a suspension of metal spheres, *Phys. Rev. B* 39 (1989) 9852–9858.
- [25] M. T. Prinkey, A. Lakhtakia, B. Shanker, On the extended Maxwell–Garnett and the extended Bruggeman approaches for dielectric-in-dielectric composites, *Optik* 96 (1994) 25–30.
- [26] A. Lakhtakia, J. A. Polo Jr., Morphological influence on surface-wave propagation at the planar interface of a metal film and a columnar thin film, *Asian J. Phys.* 17 (2008) 185–191. (The value of  $\text{Im} [\chi]$  for  $\chi_v = 5^\circ$  presented in Table 1 should be 0.0108.)
- [27] E. Kretschmann, H. Raether, Radiative decay of nonradiative surface plasmons excited by light, *Z. Naturforsch. A* 23 (1968) 2135–2136.
- [28] A. Lakhtakia, Surface-plasmon wave at the planar interface of a metal film and a structurally chiral medium, *Opt. Commun.* 279 (2007) 291–297.
- [29] H. J. Simon, D. E. Mitchell, J. G. Watson, Surface plasmons in silver film — a novel undergraduate experiment, *Am. J. Phys.* 43 (1975) 630–636.
- [30] M. A. Motyka, A. Lakhtakia, Multiple trains of same-color surface plasmon-polaritons guided by the planar interface of a metal and a sculptured nematic thin film, *J. Nanophoton.* 2 (2008) 021910.



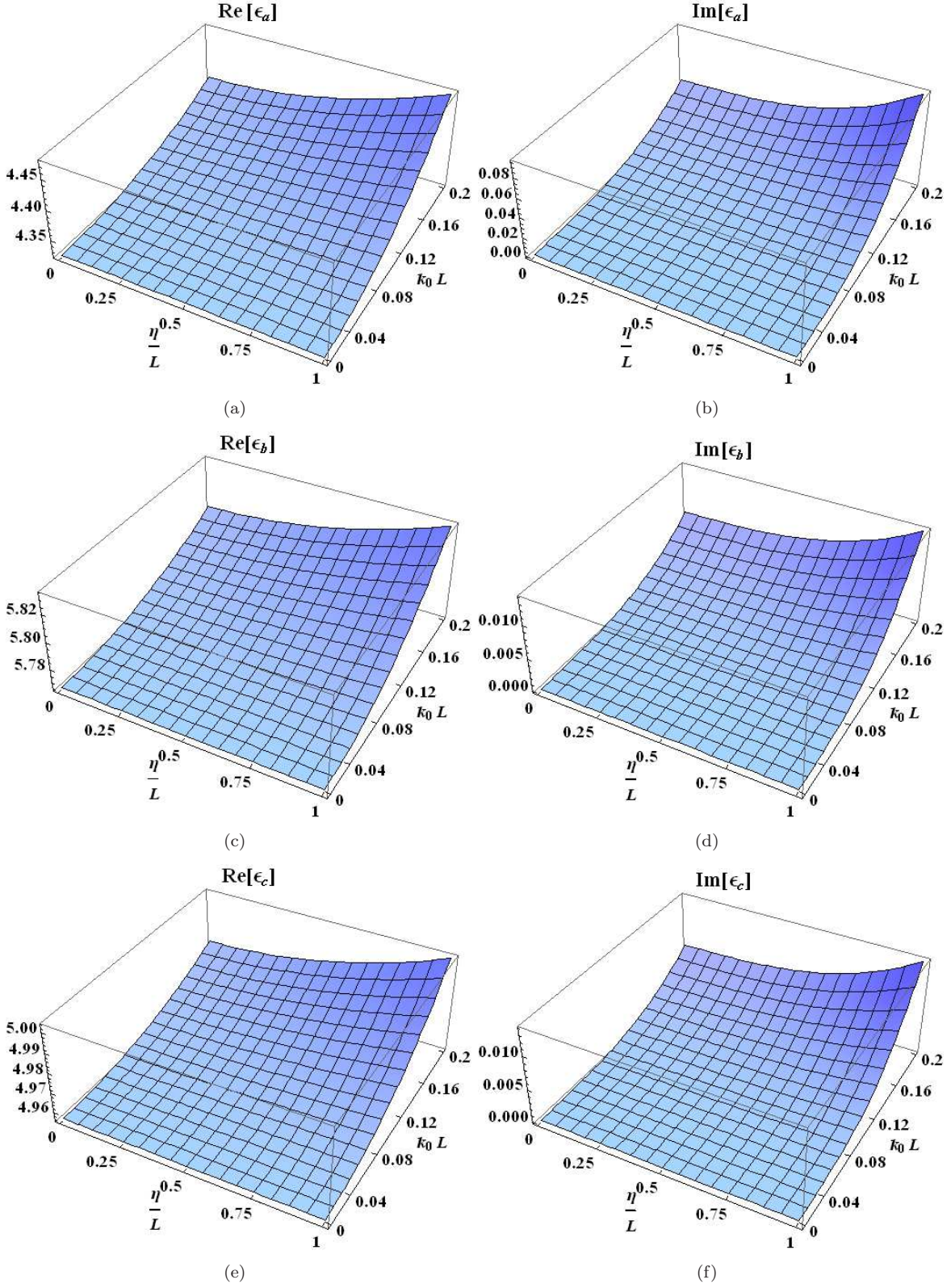


Figure 1: The relative permittivity parameters  $\epsilon_{a2}$ ,  $\epsilon_{b2}$  and  $\epsilon_{c2}$  of a fluid-infiltrated CTF, as computed using the extended second-order SPFT, plotted against  $\eta/L \in (0, 1)$  and  $k_0 L \in (0, 0.2)$ . The refractive index of the fluid infiltrating the CTF is fixed at  $n_\ell = 1.5$ .

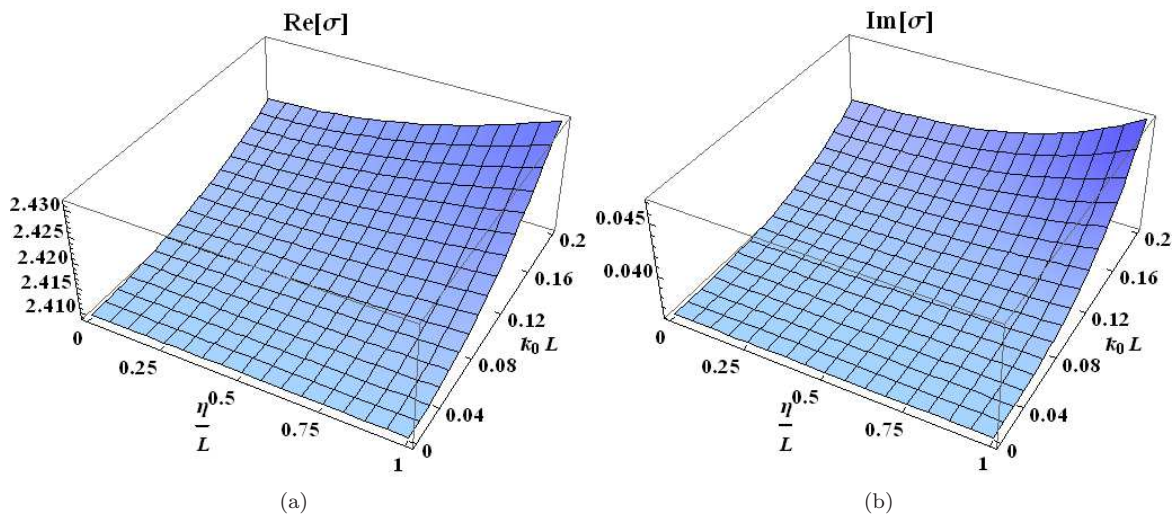


Figure 2: The real and imaginary parts of the relative wavenumber  $\sigma$  plotted against  $\eta/L \in (0,1)$  and  $k_0 L \in (0,0.2)$ .

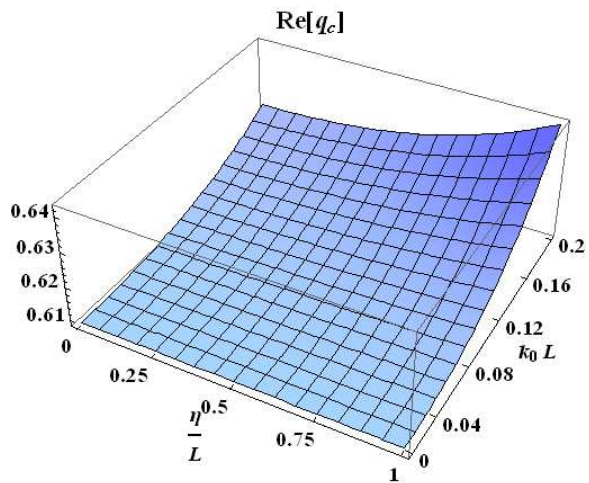


Figure 3: The real part of  $q_c$  plotted against  $\eta/L \in (0,1)$  and  $k_0 L \in (0,0.2)$ .

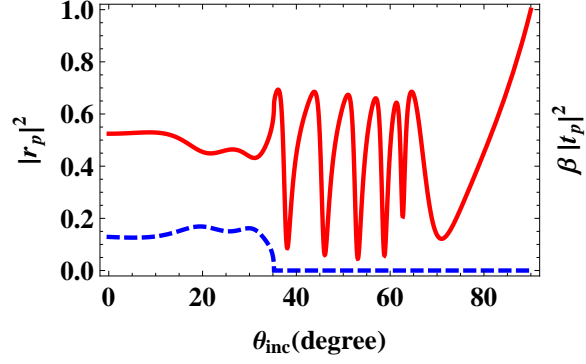


Figure 4: The reflectance  $|r_p|^2$  (red, solid curve) plotted against  $\theta_{inc}$  (in degree), for the modified Kretschmann configuration with  $\epsilon_d = 6.76$ ,  $\epsilon_m = -56 + 21i$ ,  $\epsilon_\ell = 2.25$ ,  $L_m = 10$  nm,  $L_\Sigma = L_m + 1000$  nm,  $\eta/L = 1.0$  and  $k_0L = 0.2$ . Also plotted is the quantity  $\beta |t_p|^2$  (blue, dashed curve).

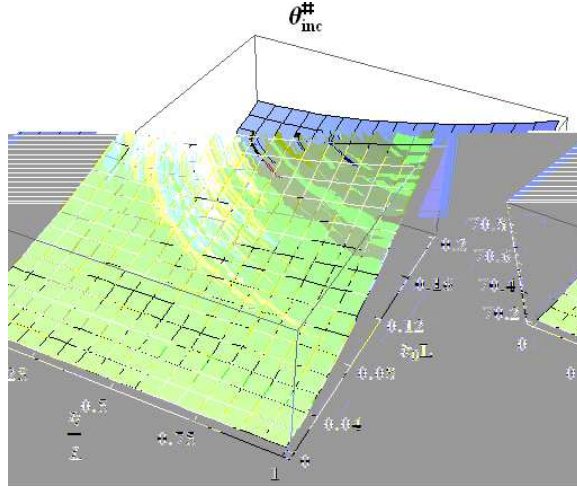


Figure 5: The angle  $\theta_{inc}^\#$  (in degree) for the scenario represented in Fig. 4, plotted versus  $\eta/L \in (0, 1)$  and  $k_0L \in (0, 0.2)$ .

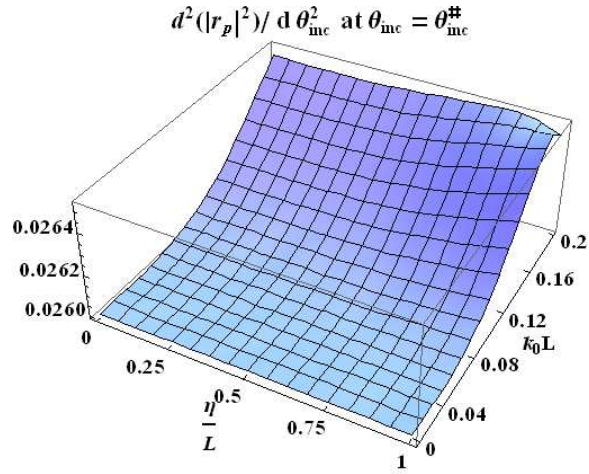


Figure 6: As Fig. 5 except that the quantity plotted is  $d^2(|r_p|^2)/d\theta_{inc}^2$  (in per degree per degree), evaluated at  $\theta_{inc} = \theta_{inc}^\#$ .

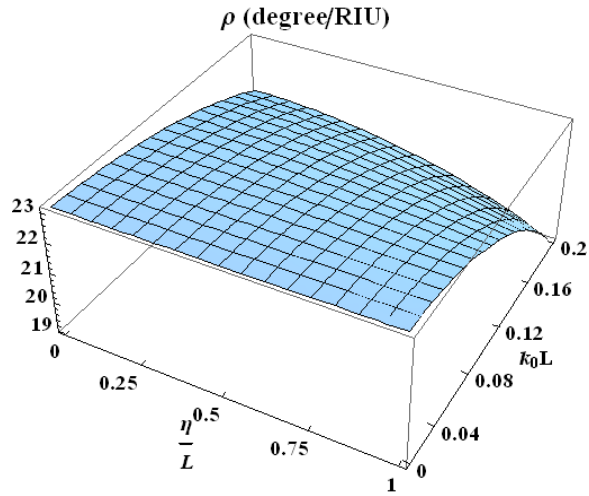


Figure 7: The figure of merit  $\rho$  (in degree/RIU) plotted against  $\eta/L \in (0, 1)$  and  $k_0 L \in (0, 0.2)$  for  $n_{\ell 2} = 1.5$  and  $n_{\ell 1} = 1.0$ .